International Research Journal of Engineering and Technology (IRJET) e-ISSN: 2395-0056
Volume: 05 Issue: 03 | Mar-2018 www.irjet.net p-ISSN: 2395-0072

Characterization of Diabetic Retinopathy Detection of Exudates in Color Fundus Images of the Human Retina

Godlin Atlas L[1], Sreeji S[2], Kumar Parasuraman[3]

[1]*Computer Science and information Technology, Maria College of Engineering and Technology, Tamil Nadu, India*
[2]*1School of Computing Science and Engineering, Galgotias University, Uttar Pradesh, India*
[3]*Center of Information Technology and Engineering, Manonmaniam Sundaranar University, Tamil Nadu, India*

Abstract - *Diabetes happens when the pancreas neglects to discharge enough insulin, gradually influencing the retina of the human eye. As it advances, the vision of a patient begins decaying, prompting diabetic retinopathy. In such manner, retinal pictures procured through fundal camera help in breaking down the results, nature, and status of the impact of diabetes on the eye. The destinations of this investigation are to (I) distinguish vein, (ii) recognize hemorrhages and (iii) group distinctive phases of diabetic retinopathy into typical, direct and nonproliferative diabetic retinopathy (NPDR). The premise of the order of various phases of diabetic retinopathy is the discovery and measurement of veins and hemorrhages introduce in the retinal picture. Retinal vascular is divided using the complexity between the veins and encompassing foundation. Discharge hopefuls were recognized utilizing thickness examination and bouncing box strategies. At long last, arrangement of the distinctive phases of eye ailment was finished utilizing Random Forests strategy in light of the territory and border of the veins and hemorrhages. The calculation has been tried on a little picture information base and contrasted and the execution of a human grader. Thus, we get a mean affectability of 92.8% and a mean prescient estimation of 92.4%. Heartiness as for changes of the parameters of the calculation has been assessed.*

Key Words: Retina, Blood Vessel, Haemorrhages, Classification, Diabetic Retinopathy

1.INTRODUCTION

Diabetes is a malady which happens when the pancreas does not emit enough insulin or the body can't process it appropriately. As diabetes advances, the infection gradually influences the circulatory framework including the retina and happens because of long haul aggregated harm to the veins, declining the vision of the patient prompting diabetic retinopathy. Following 15 years of diabetes around 10% of individuals wind up daze and roughly 2% create extreme visual impedance. As per a gauge by WHO, in excess of 220 million individuals worldwide have diabetes [1]. It is the 6th biggest reason for visual deficiency among the general population of working age in India, making it the world's diabetic capital.

Retinal pictures obtained through fundal camera with backmounted computerized camera [2] give helpful data about the outcome, nature, and status of the impact of diabetes on the eye. These pictures help ophthalmologist to assess patients with a specific end goal to design distinctive types of administration and screen the advance all the more productively [3]. The retinal microvasculature is special in that it is the main piece of human course that can be specifically envisioned non-intrusively in vivo, and can be effectively shot for computerized picture examination [2].

Prior, Otsu, (1979) [4] displayed a nonparametric and unsupervised technique for programmed limit determination for picture division. This uses just the zeroth- and the principal arrange combined snapshots of the dark level histogram. Chaudhuri et al., (1989) [5] tended to the issue of recognizing veins which have normally poor neighbourhood differentiate and accentuates that current edge recognition calculation yield unacceptable outcomes. They proposed an administrator for highlight extraction in light of optical and spatial properties of the question be perceived. Patton et al., (2006) [2] sketched out the division of retinal historic points whereupon retinal advanced picture investigation is based. Hatanaka et al., (2007) [6] portrayed an enhanced technique for identifying haemorrhages in fundus pictures. The general location plot comprised of six phases - picture digitisation, picture standardization, extraction of optic nerve head, discovery of haemorrhages competitors, end of false positives (FP) in veins, and end of FPs by highlight investigation. Be that as it may, the strategy for end of the veins for the effective discovery of discharge applicants was not managed here. Yun et al., (2008) [3] proposed programmed arrangement of various phases of diabetic retinopathy - gentle non-proliferative retinopathy, direct no proliferative retinopathy, serious non-proliferative retinopathy and proliferative retinopathy utilizing neural system from six highlights separated from the retinal pictures.

In this work, we propose another strategy for vein extraction which is a change over the already created coordinated channel, another technique for haemorrhages recognition and order the retinal cases utilizing a progressed nonparametric technique with higher grouping precision. The goals of this work are: (I) location of veins, (ii) recognition of hemorrhages, and (iii) order of the discoveries into ordinary, direct non-proliferative diabetic retinopathy (NPDR) and serious NPDR.

The paper is composed as takes after: segment II examines the proposed calculations for vein, discharge location and a short exchange on the Random Forest grouping.

Consequences of the algorithmic execution on the information are displayed in segment III, trailed by dialog and conclusions in area IV.

2. MATERIALS AND METHODS

65 retinal images of normal, moderate NPDR, and severe NPDR cases used in this work were downloaded from STARE (Structured Analysis of the Retina) Project database (http://www.parl.clemson.edu/stare/) as detailed in Table I. They were acquired in 24-bits per pixel with a dimension of 576 x 768. all possible orientations, 25 kernels of the matched filter are generated each oriented at an angle of 7.5º. The rotation matrix is given by (2)

$$\begin{bmatrix}\cos\theta & \theta i \\ -\sin i & \end{bmatrix} \quad (2)\ ri = \begin{bmatrix} \theta & \theta i \cos i \\ \sin & \end{bmatrix}$$

The filter is supposed to be centered at [0, 0]. A set of kernels are applied to fundus image and at each pixel only the maximum of their responses is retained. The corresponding weights in the kernels are given by

Table -1: Details of Retinal Diabetic Images

Type	Number of cases
Normal	30
Moderate NPDR	23
Severe NPDR	12

2.1 Blood Vessel Detection

Blood vessels can act as landmarks for localising the optic nerve, the fovea and lesions. As a result of systemic or local ocular disease, the blood vessels can have measurable abnormalities in diameter, color and tortuosity. There are three interesting properties of the blood vessels in retinal images that help in differentiating them from other features:

1) The anti-parallel pairs can be approximated by piecewise linear segments due to small curvatures present in the blood vessels.

2) Vessels have lower reflectance compared to other retinal surfaces, so they appear darker relative to the background. It was observed that these vessels almost never have ideal step edges. Although the intensity profile varies by a small amount from vessel to vessel, it may be approximated by an inverted

Gaussian curve as given by (1)

$$f\,x\,y(\ ,\ ) = -A\left\{ k \exp\left(- \frac{d\sigma 22}{} \right) \right. \qquad (1)$$

where, d = perpendicular distance between the point (x, y) and the straight line passing through the center of the of the blood vessel in a direction along its length, σ = spread of the intensity profile, A = gray level intensity of the local background, and k = measure of reflectance of the blood vessel relative to its neighbourhood.

3) Although the width of a vessel decreases as it travels radially outward from the optic disk, such a change in vessel caliber is a gradual one. The widths of the vessels are found to lie within a range of 2-10 pixels (36-180 μm).

The matched filter has the same inverted Gaussian response as the gray level profile of the blood vessel. The design of the matched filter is as follows: assuming that all blood vessels are of equal width, the Gaussian curve is truncated at u= 3± σ, u is a point in the rotated coordinate system, the length of piecewise linear segment L=17, an angular resolution of 7.5º to span u2

$$k\,x\,yi\ (A, B) = -\exp\left(- \frac{}{2\sigma 2} \right) \qquad (3)$$

Therefore,

$$\left(L \right) N = \left\{ (u\ v\ u,\ ) \,||\leq 3\sigma, |\ v\ | \leq \right\} \qquad (4)$$

If A denotes the total number of points in N then the mean is given by (5):

$$= \sum K\,x\,yi\ (\ ,\ )mi \quad (5)\ \ p\ Ni\varepsilon\ (A)$$

where mi is the mean value of the kernel and i is the kernel number. The convolutional mask of the kernel is given by (6):

$$K\,x\,yi'\ (\ ,) = K\,x\,y\ mi\ (\ ,\ \ \ ) - i \qquad (6)$$

Now, template matching can be employed to detect the blood vessel

For applying the entire algorithm of the matched filter, the G-plane of the image is considered (since it yields better results). After enhancing the contrast of the image, median filter is used to remove the noise. The designed matched filter is applied on the image to detect the blood vessels. Finally, a binarised image is obtained by thresholding. However, a major shortcoming of the whole process is the presence of discontinuous lines in the detections. To improve on this, perception based binarisation was carried out using a new binary detection method. A matrix was generated to store the number of matched filter which was responsible for detecting that particular pixel of the blood vessel. The gray level value of the pixels in a particular direction of detection was multiplied by a factor. The value was then checked to be above threshold level. For 0°, 15° and 180°, pixels in the horizontal direction were checked; for 30°, 45° and 60°, pixels in the 45 degree and 225 degree directions were checked; for 75°, 90° and 105°, pixels in vertical direction and for 120°, 135° and 150°, pixels in 135 degree and 315 degree directions were checked. If gray value multiplied by a factor (say 1.2) was greater than the threshold, then that pixel was counted as blood vessel. Finally, the blood vessels are extracted pixel by pixel.

2.2. Hemorrhage Detection

The detection scheme for hemorrhage candidates consisted of four stages: 1) image digitisation, 2) detection of hemorrhage candidates, 3) elimination of FPs (false positive) in blood vessels, and 4) elimination of FPs by feature analysis.

Due to flash light used in the fundus photography, there is a typical change in the colour of the fundus images. The brightness values of the fundus image were transformed by a nonlinear curve in the hue saturation value (HSV) space. In order to emphasise brown regions, the brightness corrected colour fundus images were then subjected to gamma correction on each red, green, and blue (R, G and B) image. The gamma value was empirically set to 1.5. Subsequently, the histograms of each R, G and B image were extended. Finally, the hemorrhage candidates were detected using density analysis. The difference in the pixel values between two smoothened images detected the blood vessels and hemorrhage candidates. The FPs blood vessels were eliminated using bounding box technique The ratio of major axis length and the minor axis length of each segment was calculated as given by (7) and those with higher values were eliminated.

$$\text{ratio} = \frac{\text{Major axis length}}{\text{Minor axis length}} \quad (7)$$

Ratios above 1.57 were eliminated and those below 1.57 were considered as hemorrhages. This concept is valid when hemorrhages are assumed to be near to round shape and the blood vessels exhibit is linear shape.

2.3 Classification

This involves three stages – (1) training stage: identifying representative training areas and developing a numerical description of the attributes of each class type through training set, (2) classification stage: data set is categorised into the class it most closely resembles, and (3) output stage: the process consists of a matrix of interpreted category types. In this work, an advanced a non-parametric Tree-type classifier – Random Forests (RF) (Breiman, 2001) is used for classification. RF are ensemble methods using tree-type classifiers

{h x(,Θk),k=1,.....,} where the{Θk}are i.i.d. random vectors and x is the input pattern. They are a combination of tree predictors such that each tree depends on the values of a random vector sampled independently and with the same distribution for all trees in the forest. It uses bagging to form an ensemble of classification tree [7-8]. RF is distinguished from other bagging approaches in that at each splitting node in the underlying classification trees, a random subset of the predictor variables is used as potential variables to define split. In training, it creates multiple Classification and Regression Tree trained on a bootstrapped sample of the original training data, and searches only across randomly selected subset of the input variables to determine a split for each node. RF utilises Gini index of node impurity to determine splits in the predictor variables. For classification, each tree casts a unit vote for the most popular class at input x. The output of the classifier is determined by a majority vote of the trees that result in the greatest classification accuracy. It is superior to many treebased algorithms, because it lacks sensitivity to noise and does not overfit. The trees in RF are not pruned; therefore, the computational complexity is reduced. As a result, RF can handle high dimensional data, using a large number of trees in the ensemble. This combined with the fact that random selection of variables for a split seeks to minimise the correlation between the trees in the ensemble, results in error rates that have been compared to those of Adaboost, at the same time being much lighter in implementation. Breiman and Cutler (2005) suggests RF "unexcelled in accuracy among current algorithms". RF has also outperformed CART and similar boosting and bagging-based algorithm [8]. In the current work, RF has been implemented using a Linux based random forest package, available in R interface (http://www.rproject.org).

2.4. Accuracy Assessment

The accuracy of the classification was done using sensitivity, specificity, positive prediction value (PPV), negative prediction value (NPV) as given by equations (8-11) based on the four possible outcomes - true positive (TP); false positive (FP), true negative (TN) and false negative (FN).

$$\text{Sensitivity} = TP / (TP + FN) \quad (8)$$
$$\text{Specificity} = TN / (FP + TN) \quad (9)$$
$$PPV = TP / (TP + FP) \quad (10)$$
$$NPV = TN / (TN + FN) \quad (11)$$

The sensitivity measures the proportion of actual positives which are correctly identified. The specificity measures the proportion of negatives which are correctly identified. PPV is the precision of positives that were correctly identified. NPV is the precision of negatives correctly identified.

3. RESULTS

In a RGB retinal image, contrast is greater when the green channel alone is utilised in fundal image feature extraction. Adaptive histogram equalisation was used to enhance the contrast of the features of interest against the background.

3.1 Blood Vessel Extraction

A 3 x 3 median filter was used to remove the random noise as displayed in Fig. 1. Blood vessels were detected (as shown in white pixels against black background in Fig. 2) after applying the designed matched filter. The matched filtered image was converted to binary equivalent with a global threshold value of 0.1490 determined empirically (Fig. 3), where presence of discontinuous lines was observed. Perception based binarization was carried out by generating a matrix, to store the matched filter number, and then the

pixel gray level in that particular direction, multiplied by a factor, was checked for a threshold level.

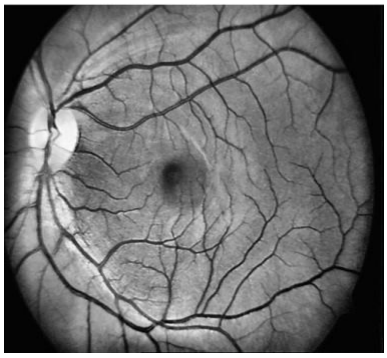

Figure 1. Retinal image after removing the noise.

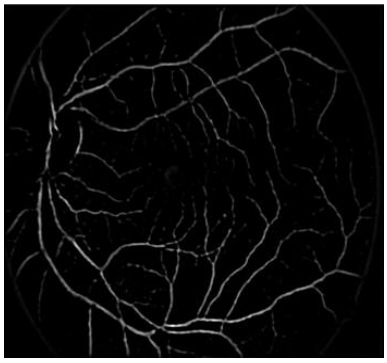

Figure 2. Image obtained after passing through the matched filter.

Figure 3. Figure 3: Binary image after thresholding.

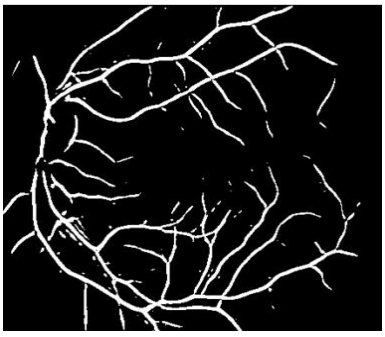

Figure 4. Image after perception based binarisation.

The pixels were examined in horizontal direction, 45°, 225°, vertical direction, 135° and 315°. If the gray value multiplied by the factor was greater than the threshold, the pixel was counted as blood vessel. Extracted blood vessels are shown as white pixels in Fig. 4. During the conditions of diabetes, the density of these vessels increases too many fold, rendering a clear indication of the development of diabetic retinopathy in the patient. The density can be estimated by finding the total area of the blood vessels i.e., the total number of white pixels in the image.

3.1 Hemorrhage Detection

Two smoothened images of different window sizes were obtained using smoothening filter and differenced to extract blood vessels and detect hemorrhage candidates. The image was thresholded using a global thresholding value as shown in the Fig. 5. The false positive blood vessels were eliminated using bounding box technique. The ratio of major axis length and the minor axis length of each segment were calculated and those with higher values (>1.57) were eliminated. The hemorrhages were detected and their density was calculated by finding the number of white pixels in the image (Fig. 6).

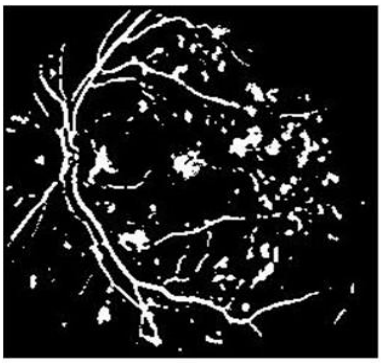

Figure 5. Thresholded image.

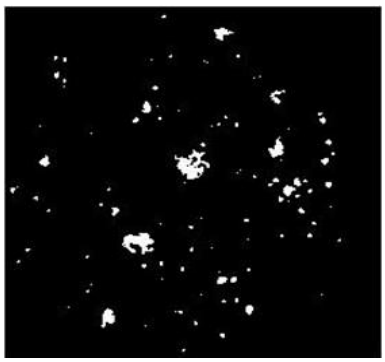

Figure 6. Hemorrhages in the retinal image.

C. Classification of different stagges of Diabetic Retinopthay
Six features – area and perimeter in each of the R, G, B components of the blood vessels and hemorrhages were extracted. Area is the number of white pixels (blood vessel and hemorrhage candidates) present within the vessels and perimeter the periphery of the vessels. These extracted features were used as inputs to the RF classifier for

categorizing the three stages of retinal images. The range of the area and perimeter values of blood vessels and hemorrhages for each stage of the diabetic retinopathy with the different RGB layers are shown in Table II and III

TABLE 2. Range of Input Area Features to Classification Algorithms

Classes	Area in R layer ($\mu\pm\sigma$)	Area in G layer ($\mu\pm\sigma$)	Area in B layer ($\mu\pm\sigma$)
Normal	9169±1529	8184±1384	8093±1467
Moderate NPDR	1269±1548	12903±1687	13365±1992
Severe NPDR	16075±1596	14879±1380	16156±1760

TABLE 3. Range of Input Perimeter Features to Classification Algorithms

Classes	Perimeter in R layer ($\mu\pm\sigma$)	Perimeter in G layer ($\mu\pm\sigma$)	Perimeter in B layer ($P_{\mu\pm\sigma}$)
Normal	5640±901	5348±840	5603±861
Moderate NPDR	7568±847	7630±725	8875±1126
Severe NPDR	9475±878	9004±552	11258±984

4. RESULTS AND DISCUSSION

The analysis revealed that TP=14, FP=0, TN=9, FN=2, sensitivity=0.875, specificity=1, positive predicted value (PPV)=1, and negative predicted value (NPV)=0.8181. The unknown test cases were classified correctly by 88.46%. This shows that the proposed method of classification based on area and perimeter of blood vessels and hemorrhages produce motivating results

Sinthanayothin et al., (2003) reported sensitivity of 80.21% and specificity of 70.66% while differentiating diabetic retinopathy from normal images. Here, the retinal images we preprocessed using adaptive, local, and contrast enhancement. They adopted a neural network based classification

- Erosion: $\left[\varepsilon^{(sB)}(f)\right](x) = \min_{b\in sB} f(x+b)$.
- Dilation: $\left[\delta^{(sB)}(f)\right](x) = \max_{b\in sB} f(x+b)$.
- Opening: $\gamma^{(sB)}(f) = \delta^{(sB)}\left[\varepsilon^{(sB)}(f)\right]$.
- Closing: $\phi^{(sB)}(f) = \varepsilon^{(sB)}\left[\delta^{(sB)}(f)\right]$.

We call sB structuring element B of size s. Furthermore, we define the geodesic transformations of an image f (marker) and a second image g (mask)

$$\varepsilon_g^{(n)}(f) = \varepsilon_g^{(1)}\varepsilon_g^{(n-1)}(f) \text{ with } \varepsilon_g^{(1)}(f) = \varepsilon^{(B)}(f) \vee g$$
$$\delta_g^{(n)}(f) = \delta_g^{(1)}\delta_g^{(n-1)}(f) \text{ with } \delta_g^{(1)}(f) = \delta^{(B)}(f) \wedge g$$
$$R_g(f) = \delta_g^{(i)}(f) \text{ with } \delta_g^{(i)}(f) = \delta_g^{(i+1)}(f);$$
$$R_g^*(f) = \varepsilon_g^{(i)}(f) \text{ with } \varepsilon_g^{(i)}(f) = \varepsilon_g^{(i+1)}(f);$$

$\varepsilon_g^{(n)}(f)$, $\delta_g^{(n)}(f)$, $R_g(f)$ and $R_g^*(f)$ are called geodesic

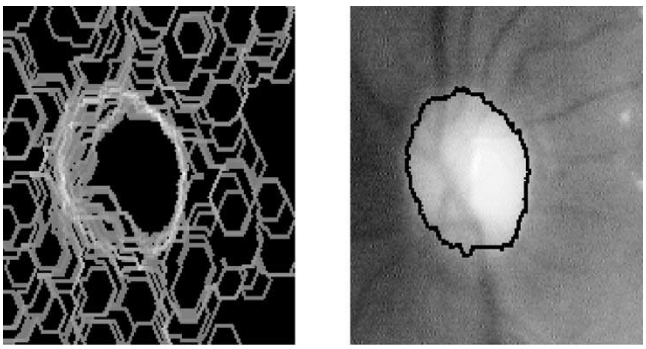

Figure 7. Area values of blood vessels and hemorrhages in RGB layers.

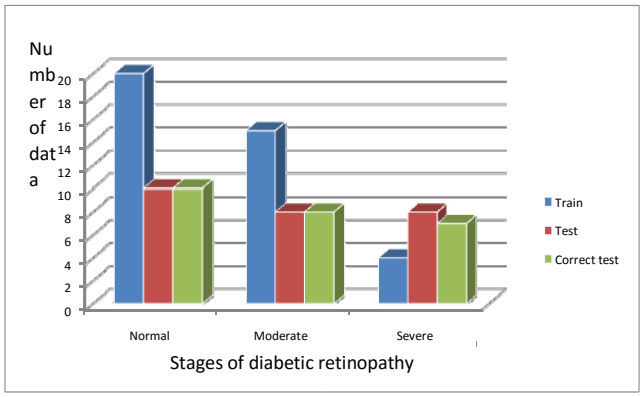

Figure 8. Graphical representation of training and testing data set for RF classifiers.

The box plots of the area and perimeter ranges of the extracted features for different kinds of images are shown in Fig. 7 and 8. The box plot function in R statistical software provided comparisons between each stage of diabetic retinopathy. For the purpose of training and testing the classifiers, the 65 retinal images were divided into two sets – a training set of 39 arbitrary samples and a test set of 26 samples. A graphical representation of training and testing data set, and the number of testing .

Similar results have been reported by Larsen et al., (2003), where hemorrhages and microaneurysms were detected to diagnose diabetes. Their method had 71.4% specificity and 96.7% sensitivity in detecting diabetic retinopathy. The results obtained from our method of feature extraction and classification scheme revealed that normal cases were classified with 90% accuracy while

5. CONCLUSION

The analysis revealed that TP=14, FP=0, TN=9, FN=2, sensitivity=0.875, specificity=1, positive predicted value (PPV)=1, and negative predicted value (NPV)=0.8181. The unknown test cases were classified correctly by 88.46%. This shows that the proposed method of classification based on area and perimeter of blood vessels and hemorrhages produce motivating results.

REFERENCES

[1] C.Sinthanayothin,J.F.Boyce,H.L.Cook,andT.H.Williamson ,"Automated localization of the optic disc, fovea and retinal blood vessels from digital color fundus images," Br. J. Opthalmol., vol. 83, pp. 231–238, Aug. 1999.

[2] Osareh, M. Mirmehdi, B. Thomas, and R. Markham, "Automatic recognition of exudative maculopathy using fuzzy c-means clustering and neural networks," in Proc. Medical Image Understanding Analysis Conf., July 2001, pp. 49–52.

[3] M. H. Goldbaum, N. P. Katz, S. Chaudhuri, M. Nelson, and P. Kube, "Digital image processing for ocular fundus images," Ophthalmol. Clin. North Amer., vol. 3, Sept. 1990.

[4] T. Walter, "Détection de Pathologies Rétiniennes à Partir d'Images Couleur du Fond d'œil," Rapport d'avancement de thèse, Ecole des Mines de Paris, Centre de Morphologie Mathématique, Paris, France, 2000.

[5] M. J. Cree, J. A. Olson, K. C. McHardy, P. F. Sharp, and J. V. Forrester, "The preprocessing of retinal images for the detection of fluorescein leakage," Phys. Med. Biol., vol. 44, pp. 29–308, 1999.

[6] E. Peli and T. Peli, "Restoration of retinal images obtained through cataracts," IEEE Trans. Med. Imag., vol. 8, pp. 401–406, Dec. 1989.

[7] B. Laÿ, "Analyze Automatique des Images Angiofluorographiques au Cours de la Rétinopathie Diabétique,", Ecole Nationale Supérieure des Mines de Paris, Centre de Morphologie Mathématique, Paris, France, 1983.

[8] T. Spencer, R. P. Phillips, P. F. Sharp, and J. V. Forrester, "Automated detection and quantification of microaneurysms in fluorescein angiograms," Graefe's Arch. Clin. Exp. Ophtalmol., vol. 230, pp. 36–41, 1991.

[9] J. Frame, P. E. Undill, M. J. Cree, J. A. Olson, K. C. McHardy, P. F. Sharp, and J. F. Forrester, "A comparison of computer based classification methods applied to the detection of microaneurysms in ophtalmic fluorescein angiograms," Comput. Biol. Med., vol. 28, pp. 225–238, 1998.

[10] F. Zana, "Une Approche Morphologique Pour les Détections et Bayesienne Pour le Recalage d'Images Multimodales: Application aux Images Rétiniennes,", Ecole Nationale Supérieure des Mines de Paris, Centre de Morphologie Mathématique, Paris, France, 1999.

[11] S. C. Lee, E. T. Lee, R. M. Kingsley, Y. Wang, D. Russell, R. Klein, and A. Wanr, "Comparison of diagnosis of early retinal lesions of diabetic retinopathy between a computer system and human experts," Graefe's Arch. Clin. Exp. Ophtalmol., vol. 119, pp. 509–515, 2001.

[12] R. Phillips, J. Forrester, and P. Sharp, "Automated detection and quantification of retinal exudates," Graefe's Arch. Clin. Exp. Ophtalmol., vol. 231, pp. 90–94, 1993.

[13] N. P. Ward, S. Tomlinson, and C. J. Taylor, "Image analysis of fundus photographs – The detection and measurement of exudates associated with diabetic retinopathy," Ophthalmol., vol. 96, pp. 80–86, 1989.

[14] K. Akita and H. Kuga, "A computer method of understanding ocular fundus images," Pattern Recogn., vol. 15, no. 6, pp. 431–443, 1982.

[15] S. Tamura and Y. Okamoto, "Zero-crossing interval correction in tracing eye-fundus blood vessels," Pattern Recogn., vol. 21, no. 3, pp. 227–233, 1988.

[16] S. Chaudhuri, S. Chatterjee, N. Katz, M. Nelson, and M. Goldbaum, "Detection of blood vessels in retinal images using two-dimensional matched filters," IEEE Trans. Med. Imag., vol. 8, pp. 263–269, Sept. 1989.

[17] Pinz, M. Prantl, and P. Datlinger, "Mapping the human retina," IEEE Trans. Med. Imag., vol. 1, pp. 210–215, Jan. 1998.

[18] F. Z. and J.-C. Klein, "Segmentation of vessel like patterns using mathematical morphology and curvature evaluation," IEEE Trans. Image Processing, vol. 10, pp. 1010–1019, July 2001.

[19] T. Walter and J.-C. Klein, "Segmentation of color fundus images of the human retina: Detectionof theoptic discandthevascular treeusingmorphological techniques," in Proc. 2nd Int. Symp. Medical Data Analysis (ISMDA 2001), Oct. 2001, pp. 282–287.

[20] F. Mendels, C. Heneghan, and J.-P. Thiran, "Identification of the optic disk boundary in retinal images using active contours," in Proc. Irish Machine Vision Image Processing Conf. (IMVIP'99), Sept. 1999, pp. 103–115.

[21] F. Z. and J.-C. Klein, "A multi-modal segmentation algorithm of eye fundus images using vessel detection and hough transform," IEEE Trans. Med. Imag., vol. 18, May 1999.

[22] P. Soille, Morphological Image Analysis: Principles and Applications. New York: Springer-Verlag, 1999.

[23] J. Serra, Image Analysis and Mathematical Morphology—Theoretical Advances. London, U.K.: Academic, 1988, vol. 2.

[24] S. Beucher and F. Meyer, "The morphological approach to image segmentation: The watershed transformation," Math. Morphology Image Processing, pp. 433–481, 1993.

[25] G. H. Bresnick, D. B. Mukamel, J. C. Dickinson, and D. R. Cole, "A screening approach to the surveillance of patients with diabetes for the presence of vision-threatening retinopathy," Ophthalmol., vol. 107, pp. 13–24, 2000.

[26] P. Massin, A. Erginay, and A. Gaudric, Rétinopathie Diabéthique. Paris, France: Elsevier, 2000, vol. 1.